Histochemistry and Cell Biology (2018) 150:379–393
https://doi.org/10.1007/s00418-018-1685-6

ORIGINAL PAPER

Wharton's jelly-derived mesenchymal cells as a new source for the generation of microtissues for tissue engineering applications

D. Durand-Herrera[1,2,3] · F. Campos[1,3] · B. D. Jaimes-Parra[1] · J. D. Sánchez-López[4] · R. Fernández-Valadés[3,5] · M. Alaminos[1,3] · A. Campos[1,3] · V. Carriel[1,3]

Accepted: 2 June 2018 / Published online: 11 June 2018

Abstract

Microtissues (MT) are currently considered as a promising alternative for the fabrication of natural, 3D biomimetic functional units for the construction of bio-artificial substitutes by tissue engineering (TE). The aim of this study was to evaluate the possibility of generating mesenchymal cell-based MT using human umbilical cord Wharton's jelly stromal cells (WJSC-MT). MT were generated using agarose microchips and evaluated ex vivo during 28 days. Fibroblasts MT (FIB-MT) were used as control. Morphometry, cell viability and metabolism, MT-formation process and ECM synthesis were assessed by phase-contrast microscopy, functional biochemical assays, and histological analyses. Morphometry revealed a time-course compaction process in both MT, but WJSC-MT resulted to be larger than FIB-MT in all days analyzed. Cell viability and functionality evaluation demonstrated that both MT were composed by viable and metabolically active cells, especially the WJSC during 4–21 days ex vivo. Histology showed that WJSC acquired a peripheral pattern and synthesized an extracellular matrix-rich core over the time, what differed from the homogeneous pattern observed in FIB-MT. This study demonstrates the possibility of using WJSC to create MT containing viable and functional cells and abundant extracellular matrix. We hypothesize that WJSC-MT could be a promising alternative in TE protocols. However, future cell differentiation and in vivo studies are still needed to demonstrate the potential usefulness of WJSC-MT in regenerative medicine.

Keywords Tissue engineering · Human Wharton-jelly mesenchymal cells · Human fibroblast · Microtissues · Microaggregates · Mesenchymal stem cells · Natural biomaterial

Introduction

Tissue engineering (TE) has the aim to develop bio-artificial substitutes to repair or replace damaged tissues and organs (Alaminos et al. 2006; Philips et al. 2018). To generate bio-artificial tissues by TE, three basic elements are needed: cells, biomaterials and growth factors (Carriel et al. 2014). In the last years, and based on this principle, our research group successfully combined natural biomaterials with different cells sources and generated bioengineered models of cornea (Alaminos et al. 2006), skin (Carriel et al. 2012), peripheral nerves (Carriel et al. 2013, 2014, 2017, 2015), palate (Fernandez-Valades-Gamez et al. 2016) and cartilage (Garcia-Martinez et al. 2017) with promising ex vivo and in vivo results.

Unfortunately, most of the bioengineered tissues failed to completely resemble the maturation, histological features and extracellular matrix (ECM) molecular composition of native tissues, especially when synthetic

✉ A. Campos
acampos@ugr.es

✉ V. Carriel
vcarriel@ugr.es

1 Department of Histology, Tissue Engineering Group, University of Granada, Granada, Spain

2 Doctoral Programme in Biomedicine, University of Granada, Granada, Spain

3 Instituto de Investigación Biosanitaria ibs.GRANADA, Granada, Spain

4 Division of Maxillofacial Surgery, University Hospital Complex of Granada, Granada, Spain

5 Division of Pediatric Surgery, University Hospital Complex of Granada, Granada, Spain

biomaterials are used. Therefore, it is still necessary to develop new techniques and to explore different cell sources to generate more biomimetic, natural and functional tissue structures able to improve tissue biomimicry (Zorlutuna et al. 2012). In this context, 3D microtissues (MT) can be generated as microaggregates of human cells grown in culture using three-dimensional systems. Generation of MT demonstrated to be an efficient method to produce functional 3D units for tissue engineering applications (Berneel et al. 2016; Roosens et al. 2017; Zorlutuna et al. 2012). These MT can be made using different kinds of techniques, including the use of non-adherent microchips, being agarose microchips the most commonly used (Achilli et al. 2012; Berneel et al. 2016; Napolitano et al. 2007b). MT can be fabricated with a broad range of shapes (spheres, cylinders, tubes, etc.) and sizes (Dean et al. 2007), and have demonstrated to be a useful alternative to the use of biomaterials (Fennema et al. 2013; Napolitano et al. 2007a). All these studies demonstrated that MT technique supports several cell functions and could increase the biomimicry of bioengineered substitutes (Achilli et al. 2012). In addition, this methodology was a useful tool to investigate the behavior and function of certain cells, cell adhesion dynamics, cell–cell or cell-ECM interactions, to create ex vivo models for cancer research and for pharmacological studies (Achilli et al. 2012; Edmondson et al. 2016; Napolitano et al. 2007a). In TE, the use of MT technique allowed to closely reproduce the complex microenvironment of some tissues, such as cartilage, pancreas, heart muscle, to generate organ-like pituitary glands and artificial ovaries-like structures containing active oocytes (Achilli et al. 2012; Berneel et al. 2016; Fennema et al. 2013; Krotz et al. 2010).

Despite the important advances obtained by the use of MT technique in different fields, including TE, the MT technique is still under development and needs further optimization. Previous studies demonstrated that the success of MT-formation depends on several factors, including the cells used. In this context, the generation of mesenchymal cell-based MT (MSC-MT) could be an important advance in the TE field, due to the multipotent differentiation capability of MSC, especially the umbilical cord Wharton's jelly mesenchymal stromal cells (WJSC), which are characterized by high levels of cell viability, functionally and differentiation potential (Garzon et al. 2012b, 2014b; Jaimes-Parra et al. 2017). For this reason, the main objective of this study was to evaluate the possibility to generate MSC-MT using WJSC for future use in TE and regenerative medicine. Furthermore, morphometry, cell viability and metabolism, MT-formation process and ECM synthesis were determined using phase-contrast microscopy, functional biochemical assays, and histological analyses.

Materials and methods

Cell cultures

In this study, WJSC and human fibroblasts (FIB)—these later used as control—were isolated from healthy tissue biopsies as described previously (Campos et al. 2017, 2016; Davies et al. 2017; Garzon et al. 2012b; Jaimes-Parra et al. 2017). Briefly, WJSC were isolated from full-term newborns umbilical cord segments in which the amniotic membrane and umbilical cord blood vessels were carefully removed as previously reported (Davies et al. 2017). Remaining Wharton's jelly perivascular tissue was mechanically fragmented, digested in a collagenase type I solution (Gibco BRL, life technologies) and cells were harvested by centrifugation. Human FIB were obtained from healthy oral mucosa biopsies from which small fragments of the connective tissue were obtained, fragmented and digested as described above. WJSC were cultured using commercially available Amniomax™ culture media (Gibco, BRL, technologies) as described previously (Garzon et al. 2012b; Jaimes-Parra et al. 2017), while FIB were cultured in Dulbecco's modified Eagle's medium (DMEM) supplemented with 1% of antibiotics solution and 10% of bovine fetal serum (Campos et al. 2017, 2016). Both cells types were kept under standard culture conditions (37 °C and 5% CO_2), the culture medium was renovated every 3 days, and the confluency was daily controlled by phase-contrast microscopy. Subconfluent cells were detached with trypsin–EDTA (Sigma-Aldrich) and subcultured in new culture flasks. Both cell types were expanded until the fifth passage, which allowed us to obtain enough number of cells for MT generation and to perform all studies in triplicate. In this study, the presence of well-known mesenchymal stem cell markers in WJSC was determined by flow cytometry as previously suggested (Dominici et al. 2006; Garzon et al. 2012b; Martin-Piedra et al. 2014). We used the BD Stemflow™ kit (Human MSC Analysis Kit, BD Biosciences) and a FACSCalibur flow cytometer (Becton, Dickinson and Company, Franklin Lakes, NJ, USA). Human WJSC used in the study demonstrated to be positive for CD73 (99.1%), CD90 (94.2%), CD105 (94.7%) and negative for CDs 45, 34, 11b, 19 and HLA-DR markers.

Agarose microchips fabrication and microtissues formation

To elaborate agarose microchips, type I agarose was dissolved in PBS to a final concentration of 3.5% and then autoclaved. To fabricate agarose microchips, this agarose solution was melted and added to commercially available

polydimethylsiloxane (PDMS) molds (Sigma-Aldrich) with a microsphere pattern. Each chip contains 256 microwells with a diameter of 400 µm and a depth of 800 µm. Once agarose was poured into the molds, it was allowed to jellify at room temperature, and solid microchips were harvested and stored in sterile PBS at 4 °C until their use.

For the generation of MT with WJSC and FIB (WJSC-MT and FIB-MT, respectively), sterile agarose microchips were placed for 1 h in 6 well-culture plates at 37 °C to equilibrate agarose microchips to the culture medium (Amniomax™ or DMEM). After that, the culture medium was removed and both cell types were trypsinized and seeded into the microchip (5×10^4 cells/microchips) in 190 µl of culture medium. Cells were let to settle into the microchips wells by gravity and then, more medium was added around the chips. These cell cultures were kept in standard conditions (37 °C at 5% CO_2) for 28 days.

Morphometric analyses

In this study, the formation of MT was daily controlled by phase-contrast microscopy (Nikon, Eclipse T*i*-U) during the whole experiment, and cultures were photographed at 0, 1, 2, 3, 4, 7, 14, 21 and 28 days. Photographs were analyzed with NIS Elements software (Nikon) and the area, diameter and circularity of each MT were determined. Circularity was calculated using the formula $f_{\text{circ}} = (4\pi A)/p^2$ as previously described (Roosens et al. 2017).

Evaluation of cell viability and metabolic activity

Once WJSC and FIB MT were generated, the viability, cellular metabolic activity, and irreversible cell-membrane damage were determined using live/dead (Invitrogen), WST-1 (Roche) and DNA quantification assays, respectively, as described previously (Campos et al. 2016, 2017; Rodriguez-Arco et al. 2016). These methods were applied to both cell types at 4, 7, 14, 21 and 28 days of ex vivo development (EVD). In the case of DNA quantification, data were also collected at 11, 18 and 25 days of EVD. WJSC and FIB cultured in plastic culture flasks were used as positive controls (live cells) as previously described (Campos et al. 2016; Rodriguez-Arco et al. 2016). As negative controls (dead cells), 2D-cultures from each cell type were treated with 1% Triton X-100 for 10 min (this induced irreversible cell-membrane damage).

The cell viability was evaluated with the live/dead morpho-functional assay in three independent microchips in each day of EVD. This test was done by following manufacturer recommendations and previously described protocols (Berneel et al. 2016; Garzon et al. 2012b; Martin-Piedra et al. 2014). Briefly, the culture medium was removed, washed twice with PBS and MT in the microchips were incubated with the working solution live/dead (calcein AM and ethidium homodimer-1) for 30 min. The solution was removed, MT were washed with PBS and then observed with fluorescent microscopy. Due to the spheroid shape of the MT generated in this study, it was not possible to perform quantitative analyses of viable (green fluorescence) and death cells (red nuclei fluorescence).

The cellular metabolic activity of MT-forming cells was quantitatively assessed with the water-soluble tetrazolium salt-1 (WST-1) colorimetric biochemical assay (Roche Diagnostics) which measures the mitochondrial dehydrogenase activity (MDA). This assay was performed according to the manufacturer recommendations and previously described protocols (Campos et al. 2016, 2017). Briefly, MT were incubated with the working solution reagent for 4 h at 37 °C. After this period, the solution was harvested and analyzed with a spectrophotometer (ASYS UVM340) and DigiRead software, both from the same manufacturer (Biocrom Ltd., Cambridge, UK). The WST-1 assay was performed in triplicate, and values were normalized to the mean values obtained from positive (100%) and negative (0%) controls.

The irreversible cell membrane damage was determined by quantifying the DNA-released to the supernatant culture medium as previously described (Campos et al. 2016, 2017; Rodriguez-Arco et al. 2016). Culture medium was collected in Eppendorf vials and DNA was measured using NanoDrop 2000. Analyses were performed in triplicate and values were normalized to the positive (0%) and negative (100%) controls, respectively.

Histological and histochemical analysis

For histological analysis of the MT, culture medium was removed and MT were harvested from the microchips with PBS (Berneel et al. 2016; Roosens et al. 2017). The PBS containing MT was collected in Falcon tubes, centrifuged and then fixed in 10% neutral buffered formaldehyde (24 h), dehydrated and paraffin-embedded following the procedure described for cell-block techniques (Carriel 2009). 5-µm thick histological sections were obtained and stained with hematoxylin–eosin (HE) for a general description, while histochemical and immunohistochemical techniques were used to evaluate the cells and ECM production. The production of acid proteoglycans was evaluated with Alcian Blue (AB) histochemical method (pH 2.5), and fibrillar collagen fibers were stained with Picrosirius Red (PS) histochemical method (Carriel et al. 2011a, b). AB stains proteoglycans in light-blue, whereas PS stains fibrillar collagens in red. Collagens type I, III and IV were detected by indirect immunohistochemistry (IHC). WJSC express specific cytokeratins (CK) as normal components of their cytoskeleton both in the native situation in the umbilical cord and under culture conditions (Garzon et al. 2014a; Jaimes-Parra et al. 2017).

For this reason, the expression of CK AE1/AE3 and CK8 was used to confirm the linage of the MT-forming WJSC, as previously suggested (Garzon et al. 2014a; Jaimes-Parra et al. 2017). All IHC staining were performed at the same time and under the same technical conditions. As a negative control of each IHC, the incubation of the primary antibody was omitted. All the technical information related to the antibodies used in this work is summarized in Table 1.

Statistical analysis

To perform correct statistical comparisons, all variables obtained from quantitative analyses were subjected to Shapiro–Wilk test of normality. In the case of area and circularity morphometric analyses, Student's *t* test was used to determine statistically significant differences. To determine the statistical differences between normalized WST-1 and DNA data, comparisons were performed using the Fischer exact test. Finally, all statistical comparisons were performed with SPSS 16.0 software and $p < 0.05$ values were considered statistically significant in a two-tailed test.

Results

MT-formation, cell viability, and morphometric analysis

The phase-contrast microscopic evaluation showed that WJSC and FIB tended to settle at the bottom of the wells during the first hours in a natural way (0 days of EVD). At this period, both cell types were observed scattered all over the micro-well bottom (Fig. 1). At 24 h, cells tended to self-assemble, and an irregular MT (microaggregate or microsphere) started to get shape. In the case of FIB, a compacted sphere was observed from 3 days of EVD onward, while WJSC formed a similar MT from day 4, although with differences (Fig. 1). In addition, MT tended to become compacted in both cell types and a size reduction apparently occurred. This phenomenon was more evident in the case of the FIB, which formed stable and more homogeneous MT over the time (Fig. 1). Strikingly, WJSC progressively released products that formed an irregular structure into the micro-well bottom and around the WJSC-based MT from day 4 onward (Fig. 1).

The live/dead cell viability test was done in well-established MT at 4, 7, 14, 21, and 28 days of EVD. Results showed that MT formed by both cell types were mainly composed of viable cells (green fluorescence) at all periods analyzed, and very few dead cells (red fluorescence) were occasionally observed. Interestingly, in WJSC-MT, a less-reactive core was progressively formed from 4 EVD onward, which suggests a progressive peripheral organization of viable cells during the MT-formation process. This particular pattern differed with respect to the homogeneous green-staining observed in FIB-MT over the time (Fig. 2). Concerning the dead cells, few red cells were observed inside the WJSC-MT from 7-EVD onward. However, red fluorescence staining was more evident in the irregular structure formed into the micro-well bottom and outside the WJSC-MT suggesting that this structure mainly consists of DNA remnants. Therefore, the irregular structure generated by WJSC between 4 and 28 days of EVD could mostly correspond to cellular debris (Fig. 2).

The morphometric analyses confirmed the progressive compaction and size reduction (area in μm^2) in both MT over the time. However, the area of FIB-MT was significantly lower ($p < 0.05$) than WJSC-MT in each day of EVD (Fig. 3). The evaluation of the circularity revealed that MT from both cell types tended to acquire a progressively more circular shape, especially FIB-MT, which showed significantly higher circularity values ($p < 0.05$) as compared to

Table 1 Technical details for each antibody used in this study

Antibodies	Technical information of the IHC procedures		
	Dilution/incubation	Pretreatment	References
Mouse anti-cytokeratin monoclonal (clone AE1/AE3)	Ready to use 60 min	EDTA buffer pH 8 PT-Module (95 °C)	Master Diagnóstica. Spain No. MAD-001000QD
Rabbit anti-cytokeratin 8 monoclonal (clone EP17)	Ready to use 60 min	EDTA buffer pH 8 PT-Module (95 °C)	Master Diagnóstica. Spain No. MAD-000683QD
Rabbit anti-collagen I polyclonal	1:500, 90 min	Pepsin 10 min at 37 °C	Acris antibodies. Germany No. R1038
Rabbit anti-collagen III polyclonal	1:250, 60 min	Citrate pH 6 PT-Module (95 °C)	ABCAM No. ab 7778
Mouse anti-collagen IV monoclonal (clone CIV22+PHM-12)	Ready to use 60 min	EDTA buffer pH 8 25 PT-Module (95 °C) and pepsin 10 min 37 °C	Master Diagnóstica. Spain No. MAD-001060QD
Horse anti-mouse IgG (peroxidase)	Ready to use 30 min	–	Vector laboratories No. MP 7402
Horse anti-rabbit IgG (peroxidase)	Ready to use 30 min	–	Vector laboratories No. MP 7401

PT-Module is an automated system for simultaneous dewaxing, hydration and antigen retrieval

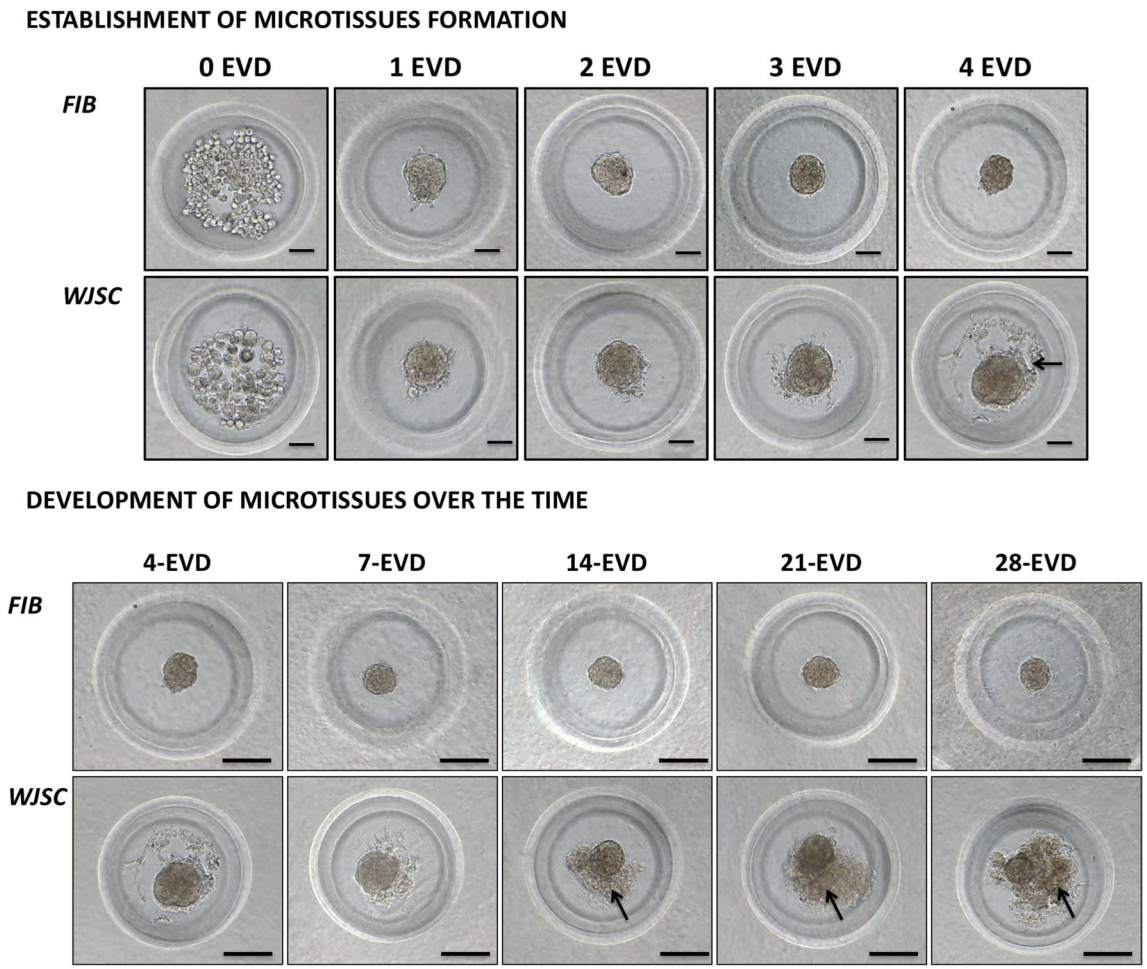

Fig. 1 Microtissue formation over the time using human oral fibroblast (FIB) and Wharton's jelly stromal cells (WJSC). During the establishment of the MT from 0 to 4 days of EVD, differences between both cell types used were evident. FIB formed a stable and compact MT, while WJSC-MT deposited an irregular structure into the micro-well bottom around the WJSC-MT (arrows). The evolution of both MT during the 28 days of EVD was characterized by compaction and size reduction, especially in WJSC-MT. For pictures from 0 to 4 days of EVD the scale bar 100 µm, while for pictures from 4 to 18 days of EVD scale bar 200 µm

WJSC-MT, which curiously from day 4 onward started to lose their circularity (Fig. 3).

Cellular metabolic activity and cell-membrane damage results

The WST-1 quantitative biochemical analysis of the MDA revealed that cells in both MT generated in this study contained metabolically active cells over the time. FIB-MT showed a mean of MDA value of 23.18%, with maximum values at days 14 (29.84%) and 21 (29.73%) of EVD (Table 2). In the case of WJSC-MT, the mean MDA value was of 47%, with maximum values at days 7 (64.92%) and 14 (63.19%) of EVD, being higher than the mean and maximum MDA values observed in FIB-MT (Table 2). Curiously, an abrupt decrease of the cellular metabolic activity occurred in WJSC-MT between 21 and 28 days of EVD, where MDA values decreased from 59.18 to 5.84% respectively, being the lower MDA values of this study (Table 2). Although FIB-MT showed lower mean MDA values than WJSC-MT, these were consistently stable over the time. Importantly, statistical analyses revealed significantly higher MDA values of both groups as compared to negative controls in each period, but MDA values were significantly lower to those observed in positive controls (2D cultured cells) (Table 2).

The quantitative analysis of the DNA-released from both MT types to the surrounding culture medium showed very low values of DNA over the time. In FIB-NT, small amounts of DNA were detected at 25 and 28 days of EVD (0.1 and 0.38%, respectively), while the percentage of DNA-released by WJSC-MT started to increase from 18 days of EVD onwards, reaching to the maximum values (5.16%) at 28 days of EVD (Table 2). Statistical analyses demonstrated that the amount of DNA-released by both MT-forming cells

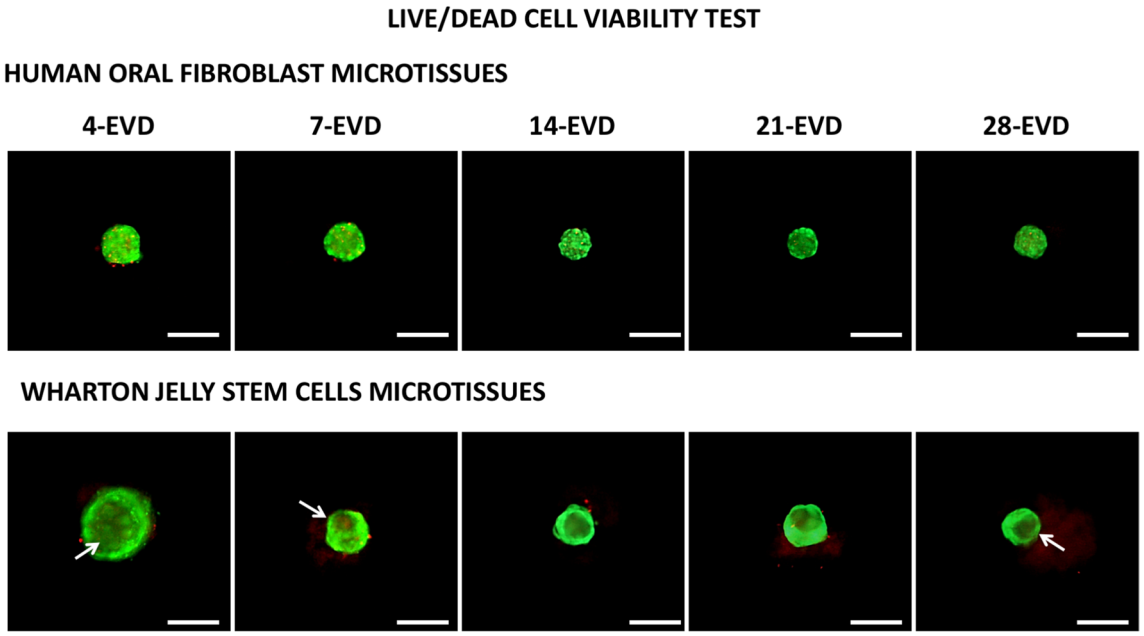

Fig. 2 Morphofunctional Live/Dead cell viability test. The cell viability was stable and high in both MT over the time. In the case of WJSC-MT, a core with less staining signal is observed (arrows). Green fluorescence indicates viable cells while red reaction indicates dead cells (DNA staining). Scale bar 200 µm

was significantly lower than negative controls, in which the total amount of DNA was released (100%). In addition, no statistically significant differences were observed between the amounts of DNA-released from both MT with respect to the values obtained in their respective positive controls (0%) (Table 2).

Histological, histochemical, and IHC results

The histological analyses carried out with HE staining showed that MT had different morphological patterns depending on the cell type and the analyzed follow-up period. Histology of FIB-MT revealed that these cells were able to generate stable MT composed of numerous fibroblasts and an eosinophilic ECM. Cells were observed homogeneously distributed inside the MT and showed prominent nuclei and a stable morphological pattern over the time with a slight decrease of the cellularity at 28 days of EVD (Fig. 4, HE staining). In addition, it was not observed any signs of apoptosis, necrosis or MT degradation, and the irregular deposition observed in WJSC-MT did not appear in the histological sections, confirming that it was not part of and it was not attached to the MT structure. On the other hand, the histology of WJSC-MT showed clear histological differences as compared to FIB-MT. During the first days, the distribution of WJSC was apparently similar to fibroblast, but from 7 days of EVD onward the WJSC adopted a clearly peripheral organization forming a multilayered capsule-like structure with an eosinophilic ECM-rich core, confirming the observations described by phase-contrast microscopy and live/dead assay. This core contained some cells at the beginning, but with the advance of the time, the number of these cells decreased and resulted in a core mainly composed by ECM molecules (Fig. 4, HE staining).

The histochemical analysis of ECM synthesis using PS staining for mature and highly organized fibrillar collagens and AB staining for acid proteoglycans suggested the production of ECM components during the formation of both MT types (Fig. 4, PS and AB). PS staining showed a moderately positive reaction for collagens in WJSC-MT, suggesting the presence of these molecules in this group. In contrast, this staining was weak and mainly negative in FIB-MT (Fig. 4, PS). Concerning the analysis of proteoglycans, AB staining showed that both cell types were able to synthesize these molecules during the MT-formation process over the time. In the case of FIB-MT, a slight intercellular pattern was observed, as well as a superficial weak positive reaction between 14 and 28 days of EVD (Fig. 4, AB). The AB histochemical staining of WJSC-MT showed that cells produced a high amount of proteoglycans as compared to FIB-MT. Interestingly, the AB positive reaction was mainly associated to the intercellular compartment. At 4 days of EVD, the AB positive reaction was broadly distributed in the MT but, with the advance of the EVD, proteoglycans remained restricted to the intercellular ECM and followed the peripheral pattern of the WJSC in the MT (Fig. 4, AB from 7 to 28 EVD).

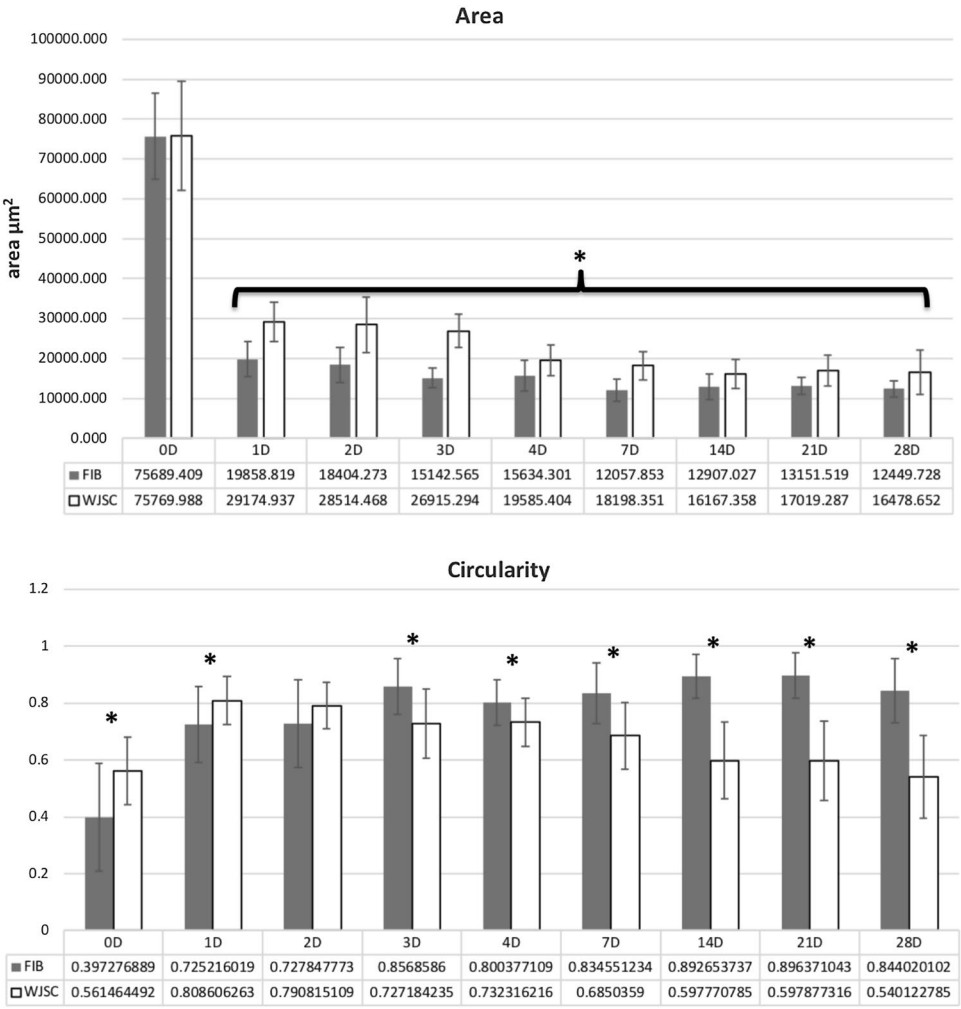

Fig. 3 Morphometric results. Top panel, analysis of the MT area demonstrating an important reduction in the area of both cell types over the time. Differences between both cells were statistically significant for each period ($p < 0.05$ for the Student *t* test). Lower panel, analysis of MT circularity revealed that WJSC-MT were initially more circular, but FIB-MT became more circular from day 3 of EVD. Differences were statistically significant for time periods labeled with asterisks (*). Note that all values were obtained from area and circularity measurement of the whole MTs (cells + inner ECM)

The IHC analysis confirmed the synthesis of different kinds of collagens by both MT-forming cells. The IHC identification of type I collagen demonstrated that WJSC and FIB were able to synthesize this molecule during MT-formation and maturation (Fig. 5, COLL I). In FIB-MT, the pattern was intercellular and strongly positive at days 21 and 28 days of EVD. In the case of WJSC-MT, collagen type I was observed with an irregular distribution among the cells and in the ECM-rich MT's core. Markedly, collagen type I showed a decrease between the 4 and 7 days of EVD, but it was followed by a progressive increase from 7 days of EVD onward (Fig. 5, COLL I from 7 to 28 EVD). The analysis of type III collagen revealed an abundant and consistent positive reaction in both MT, with a clear intercellular pattern in FIB-MT and strongly positive in the ECM-rich core produced by the WJSC (Fig. 5, COLL III). Finally, the positive reaction for type IV collagen was restricted to WJSC-MT from 4 days of EVD onward. Curiously, type IV collagen progressively acquired a basal membrane-like pattern which clearly delimited the cells from the ECM-rich core (Fig. 5, COLL IV).

To confirm the characteristic CK expression profile of the WJSC (Garzon et al. 2014a), the expression of CK AE1/AE3 and CK8 was determined. The identification of these cytokeratins showed a strongly positive reaction for WJSC-MT over the time (Fig. 6). In addition, both markers helped to confirm the progressive peripheral organization that WJSC acquired during MT-formation process, as well as, the presence of few cells in the ECM-rich MT's core (Fig. 6). In general, both markers showed a comparable cytoplasmic pattern, but the immunoreaction for CK 8 was more intense in all days of EVD analyzed (Fig. 6, CK8). As expected, both markers were negative in FIB-MT, although AE1/AE3 CK showed a weakly positive reaction for some cells at 4 days of EVD (Fig. 6, CK AE1/AE3).

Discussion

In TE, it is important to generate substitutes that should resemble the structure, cellular and ECM composition and function of specific tissues or organs (Atala 2012; Carriel

Table 2 Quantitative results of WST-1 test for mitochondrial metabolic activity and released DNA

	WST-1 (mitochondrial metabolic activity)						
	4D	7D	14D	21D	28D	N-CTR	P-CTR
FIB-MT	29.28%	27.05%	29.84%	29.73%	24.04%	0.00%	100.00%
WJSC-MT	43.68%	64.92%	63.19%	59.18%	5.84%	0.00%	100.00%
FIB-MT VS. P-CTR	0.00000*	0.00000*	0.00000*	0.00000*	0.00000*	–	–
FIB-MT VS. N-CTR	0.00000*	0.00000*	0.00000*	0.00000*	0.00000*	–	–
WJSC-MT VS. P-CTR	0.00000*	0.00000*	0.00000*	0.00000*	0.00000*	–	–
WJSC-MT VS. N-CTR	0.00000*	0.00000*	0.00000*	0.00000*	0.02893*	–	–

	DNA-RELEASED (cell membrane irreversible damage)									
	4D	7D	11D	14D	18D	21D	25D	28D	N-CTR	P-CTR
FIB-MT	0.00%	0.00%	0.00%	0.00%	0.00%	0.00%	0.11%	0.38%	100.00%	0.00%
WJSC-MT	0.07%	0.00%	0.20%	0.09%	1.52%	4.42%	4.43%	5.16%	100.00%	0.00%
FIB-MT VS. P-CTR	1.00000	1.00000	1.00000	1.00000	1.00000	1.00000	1.00000	1.00000	–	–
FIB-MT VS. N-CTR	0.00000*	0.00000*	0.00000*	0.00000*	0.00000*	0,00000*	0.00000*	0.00000*	–	–
WJSC –MT VS. P-CTR	1.00000	1.00000	1.00000	1.00000	0.49749	0.12124	0.12124	0.05938	–	–
WJSC-MT VS. N-CTR	0.00000*	0.00000*	0.00000*	0.00000*	0.00000*	0.00000*	0.00000*	0.00000*	–	–

All values were normalized with respect of both controls and expressed as percentages of activity related to positive controls. Statistically significant ($p < 0.05$) differences for the exact test of Fisher are indicated with asterisks

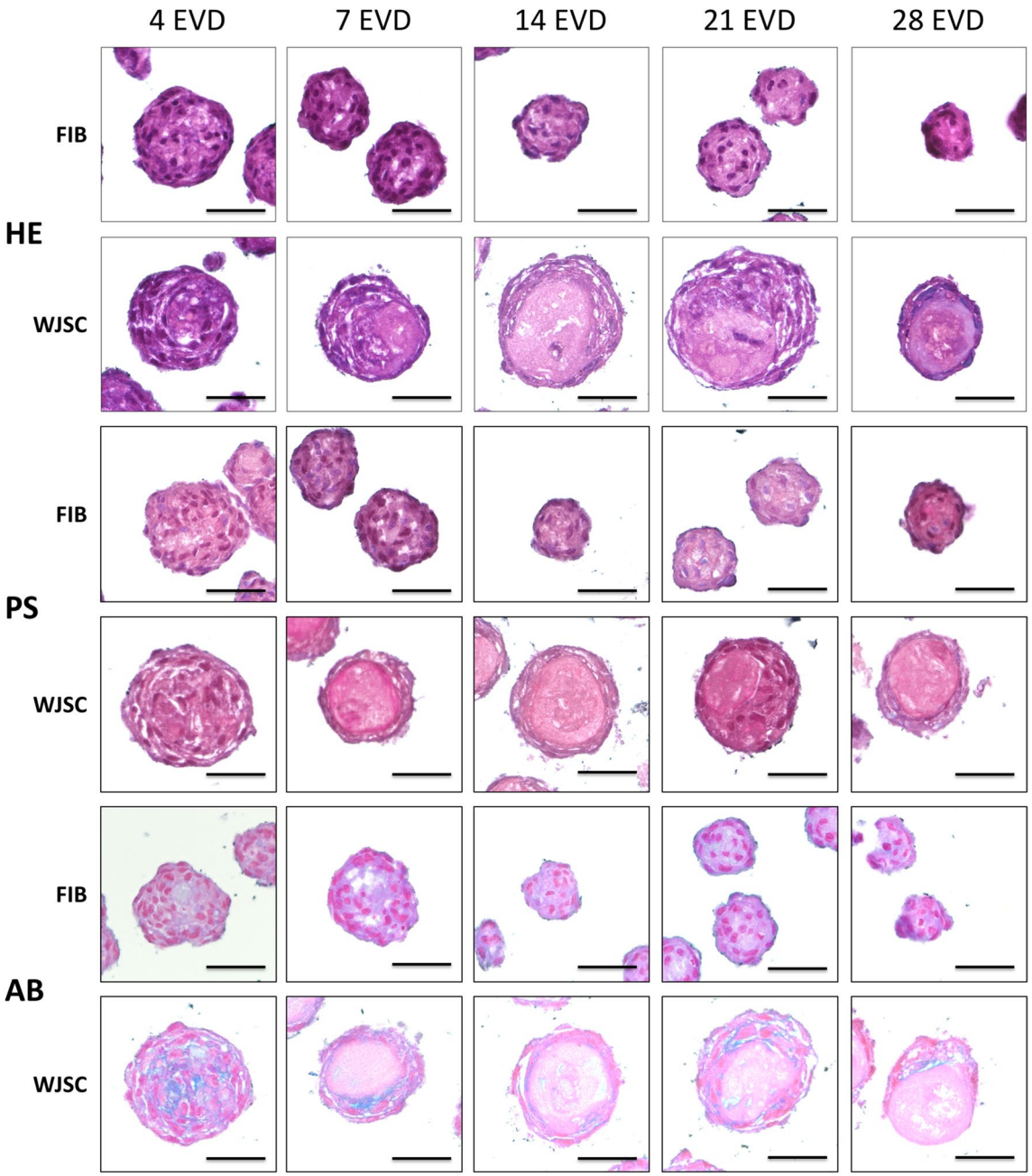

Fig. 4 Histological and histochemical analysis of FIB and WJSC-MT. The HE staining shows the morphological pattern of both MT. Picrosirius stains the fibrillar collagen fibers in red, which was preferentially observed in WJSC-MT. Alcian blue stained acid proteoglycans in light-blue in both MT. For all pictures the Scale bar 50 µm

et al. 2014; Philips et al. 2018). Currently, as it was mentioned before this is frequently achieved through the combination of cells, biomaterials and growth factors. In this context, MT technique has emerged as a promising alternative to generate scaffold-free tissue-like functional units for the construction of engineered substitutes (Fennema et al. 2013; Napolitano et al. 2007b; Roosens et al. 2017). In this regard, it would be logical to work with native adult differentiated cells, but they have several well-known drawbacks (e.g., limited expansion, dedifferentiation, difficult isolation and culture, etc.) which drives researchers to use MSC as an alternative for the generation of MT (Al Madhoun et al. 2016; Potier et al. 2016). In this study, we evaluated the possibility to generate WJSC-based MT for TE applications. For the generation of these MT, we used agarose-based microchips to stimulate cells to establish cell–cell interactions and ECM production using a previously described procedure (Berneel et al. 2016; Napolitano et al. 2007a; Roosens et al.

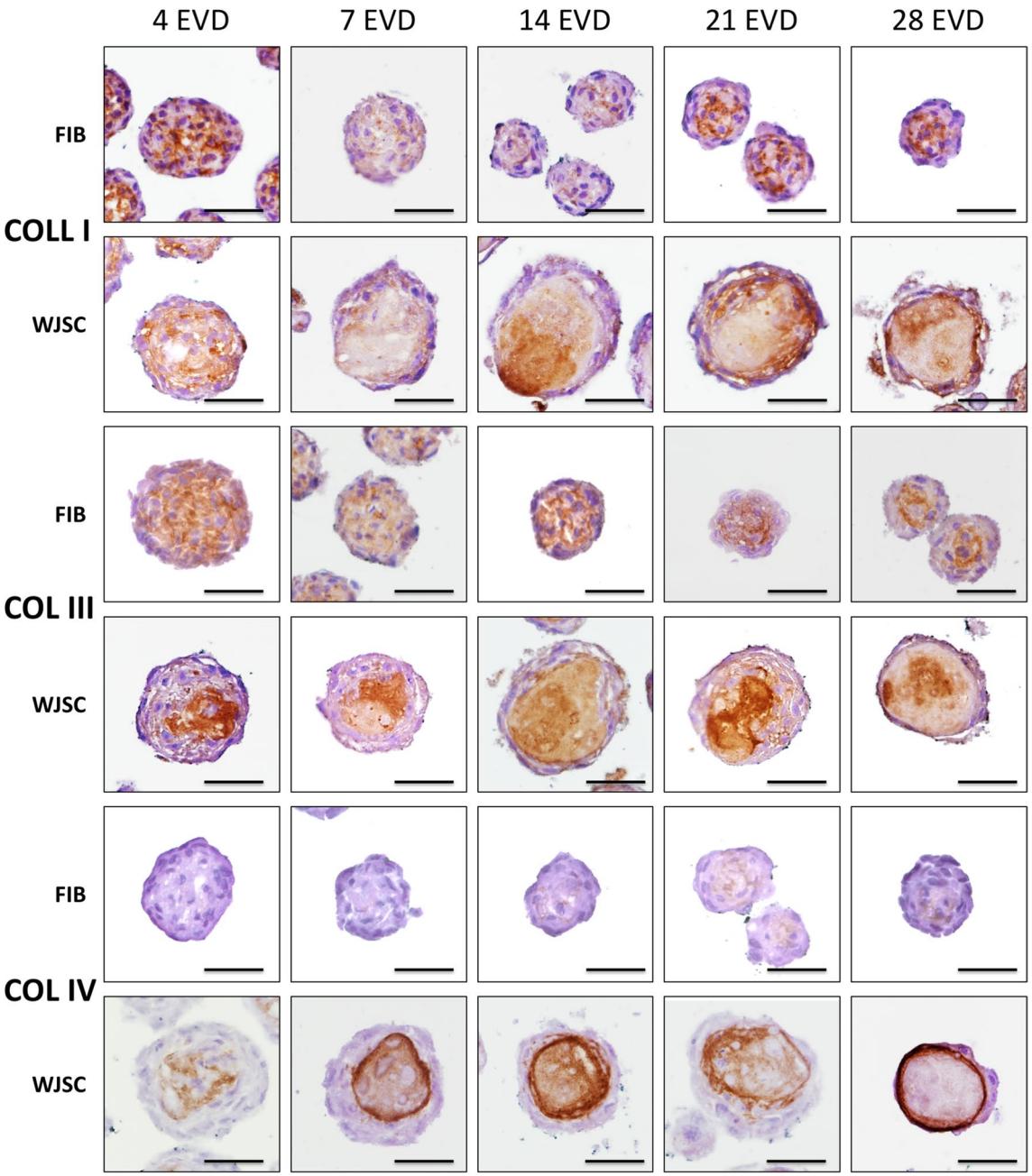

Fig. 5 Collagen type I, III and IV IHC expression in FIB-MT and WJSC-MT. Figures show the progressive synthesis of different kinds of collagens by both cells types during MT-formation and maturation. Scale bar 50 µm

2017; Song et al. 2016). MT were generated with WJSC and FIB (as control) and subjected to morphometric, cell viability, and functionality, and histological analyses.

For this study, WJSC were chosen to generate MT due to their well-known biological properties: high cell viability and functionality in culture, multipotent differentiation potential, high capacity for cell renewal, low immunogenicity, and their capability to produce a wide range of ECM molecules ex vivo (Davies et al. 2017; Garzon et al. 2012b; Jaimes-Parra et al. 2017; Taghizadeh et al. 2011). The cells used in the present study fulfilled the requirements for the use of these cells in research, including the flow cytometry characterization for typical MSC markers (CD73, 90 and 105) (Dominici et al. 2006; Garzon et al. 2012b; Martin-Piedra et al. 2014; Schugar et al. 2009), along with the positive expression of CKAE1/AE3 and CK8. Future studies are still needed to demonstrate the multipotent differentiation potential of the WJSC-MT described in this study.

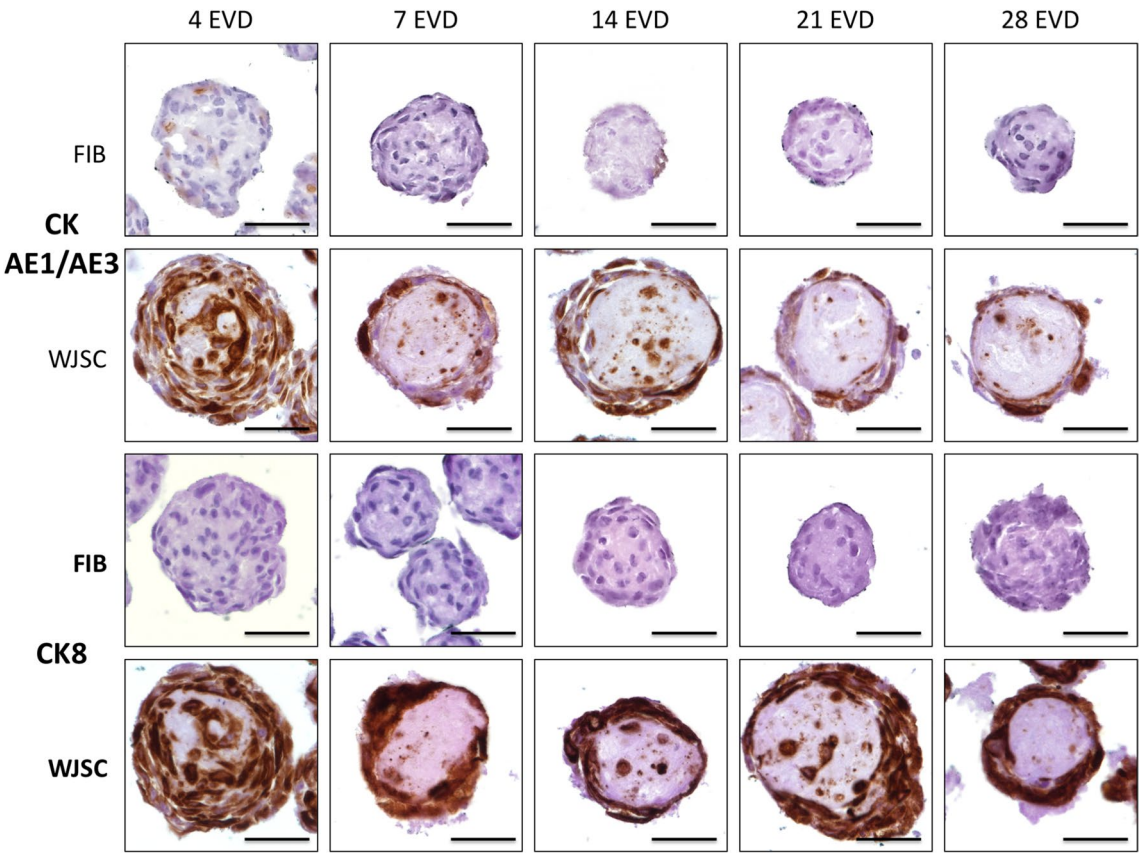

Fig. 6 Immunohistochemical expression analysis of the cytokeratins AE1/AE3 and CK8 in FIB and WJSC-MT. This IHC confirms the stable expression of these cytokeratins by MT-forming WJSC over the time. In addition, it shows the presence of few cells in the ECM core. Scale bar 50 µm

In relation to the suitability of WJSC for the generation of MT, this method was previously explored by other authors. In this sense, WJSC cultured on AggreWell plates were able to form 3D spheroid structures in 24 h and were then used to generate endoderm-like 3D spheroids with promising results (Al Madhoun et al. 2016). In addition, using hanging drop techniques, WJSC-based aggregates were used to explore the possibility to generate strategies for liver TE (Talaei-Khozani et al. 2015). These preliminary studies demonstrated the capability of WJSC to form aggregates under culture conditions and to differentiate to other cell lineages. However, the evolution of the MT or microaggregates formation, their viability and functionality profile, the histological pattern and ECM production of WJSC-based MT remain unstudied. In this regard, our study demonstrated that WJSC were able to generate stable and uniform MT under culture conditions in less than 1 week, as well as the FIB-MT used as a control. The morphometric analyses, area and circularity revealed that WJSC and FIB may have comparable behaviors during MT-formation. In both cases, the MT generation process was characterized by the progressive establishment of cell–cell interaction and compaction (area reduction), which resulted in the formation of MT from 24 h onwards. This compaction process was accompanied by the acquisition of a more circular and well-defined 3D structure. This is in agreement with previous studies where spheroidal MT underwent a compaction process which finally resulted in relatively circular 3D structures (Berneel et al. 2016; Napolitano et al. 2007b; Roosens et al. 2017).

An important aspect of any artificial tissue is the viability and functionality of the cells used (Carriel et al. 2015; Garzon et al. 2012a, b; Martin-Piedra et al. 2014). In this study, the evaluation of these parameters by live/dead and DNA-release quantification techniques demonstrated that WJSC and FIB MT mainly contained viable cells. Interestingly, live/dead assay also revealed the progressive formation of a less-reactive core in WJSC-MT, which was different to the homogeneous green-staining pattern observed in the FIB-MT (control). These findings suggest that WJSC progressively acquired a well-defined peripheral 3D organization pattern during MT-formation process, which will be discussed furtherly.

In addition, in WJSC-MT live/dead staining showed a progressive red fluorescence reaction between 21 and

28 days of EVD, which correlates with the irregular structure observed by phase-contrast microscopy. From a technical standpoint, the ethidium bromide component of the live/dead kit is an intercalant fluorochrome used to stain dead by specifically binding to A-T molecular interactions of the DNA (Kiernan 2008). We, therefore, hypothesize that this irregular structure may correspond to a progressive deposition of cellular debris containing DNA into the micro-well bottom in WJSC-MT. The progressive deposition of cellular debris with DNA could explain the slight increase of DNA which was detected from 14 to 28 days of EVD in WJSC-MT. Although a certain amount of DNA was released during MT-formation process, the maximum values for both MT were observed at 28 days of EVD, and these values only represented 0.38% of the control for FIB-MT and 5.16% for WJSC-MT. In this context, the results obtained with live/dead and DNA assays suggest that the MT-formation process has a slight impact on cell viability, which started around 21 days of EVD onward. However, this impact is not comparable to the intense effect that some biomaterials could elicit on cellular viability and functionality. For example, when human oral mucosa fibroblasts were cultured on top of genipin or glutaraldehyde cross-linked hydrogels the percentages of DNA-released reached 13 and 80% of the controls after 48 h (Campos et al. 2016, 2017). In addition, when the MDA was biochemically assessed using the WST-1 assay, this method revealed high levels of cellular metabolic activity in WJSC-MT as compared to FIB-MT. These findings are supported by previous studies demonstrating that cultured WJSC are characterized by a high proliferation capability and active metabolism (Donders et al. 2018; Garzon et al. 2012b; Jaimes-Parra et al. 2017).

In this study, WST-1 values were especially high from days 4–21 of EVD, but an important decrease occurred between days 21 and 28 days of EVD. Interestingly, the progressive increase of WST-1 values followed by an important decrease at 28 days of EVD coincided with the progressive slight increase of DNA-released values, the MT-compaction process and the progressive deposition of cellular debris containing DNA. Overall, these results suggest that WJSC may rapidly establish cell–cell interactions and generate stable, well-formed and relatively bigger MT between 4 and 21 days of EVD. However, after this period, the cell viability, functionality and structure of these MT began to be compromised. For these reasons, we would recommend not to allow the WJSC-MT to mature for long time periods under culture conditions. Instead, and to ensure the maximum levels of viable and metabolically active cells in the WJSC-MT, these structures should be generated and kept in culture for a time period ranging between 4 and 21 days of EVD. Nevertheless, future studies are still needed to determine the exact proliferation rate and the cellular mechanism which could be related to the decrease of cell viability and functionality of WJSC-MT over the time.

The histological analysis of the WJSC and FIB MT revealed the cellular 3D organization and ECM production during 28 days of EVD. Concerning the 3D organization of the cells during MT-formation process, histology demonstrated that WJSC from 7 days of EVD onward started to acquire a peripheral distribution which was clearly evident between 14 and 28 days of EVD. In this context, WJSC-MT resulted to be composed by a cellular-rich surface and a well-defined eosinophilic ECM-rich core. WJSC-MT pattern was not comparable to the consistent homogeneous distribution observed in FIB-MT. Furthermore, histology did not reveal any signs of necrosis in the MT, and also confirmed that the irregular structure associated to WJSC-MT did not form part of the MT. All this would support the hypothesis that WJSC released cellular debris during MT-formation process. Regarding the MT dimensions and structure, histology confirmed the progressive compaction process associated to a size reduction in both MT generated. However, and despite this general reduction of the MT size, the WJSC-MT resulted to be larger than FIB-MT used as control.

Regarding the structure of the MT, a recent study published by Song and cols. highlighted the importance of the cell proliferation rate on cell self-organization during microaggregate formation. In fact, they demonstrated that inhibition of cell proliferation produced by mitomycin C induced the establishment of a central core in cellular microaggregates. However, this phenomenon was not observed when cells were allowed to proliferate in the absence of mitomycin C (Song et al. 2016). In consequence, a possible explanation to the peripheral organization adopted by the WJSC in our study could be a high proliferation rate of these cells, which was previously demonstrated by other authors (Donders et al. 2018; Jaimes-Parra et al. 2017). Although we did not analyze the number of cells in each type of MT in the present study, results obtained by WST-1 analysis suggest that the metabolic activity of WJSC-MT is higher to that of FIB-MT, which could support this hypothesis. However, another possibility could be that WJSC-MT could synthetize higher amounts of ECM components could induce the cells to move to peripheral areas of the MT. Future works should clarify this issue.

Histochemical and immunohistochemical analyses of the ECM demonstrated that both cell types were able to synthesize collagens and proteoglycans during the MT-formation process. Nevertheless, the amount and spatial distribution of these components greatly differed between WJSC-MT and FIB-MT. The analysis of collagens by PS suggested the synthesis of these fibrillar components of the ECM, which was confirmed by IHC. The IHC identification of type I and III collagens confirmed that the core of WJSC-MT was mainly composed by these molecules, whereas these collagens were

broadly distributed in the FIB-MT. Interestingly, the analysis of type IV collagen revealed that this component was specific of WJSC-MT and completely absent in FIB-MT. Type IV collagen first appeared within the formation of the ECM-rich core, but with the advance of the EVD, this molecule was found as a thin, well-defined membrane-like structure. This way, type IV collagen established a clear division between the cells that make up the surface of the MT and the inner ECM-rich core. The presence of type IV collagen with this particular pattern suggests that WJSC were able to generate a basal membrane-like structure, which probably serves to attach the cells to the ECM-rich core. It is important to mention that basal membranes are not exclusive of epithelial tissues. In fact, similar structures can be found as normal components of several native tissues, such as muscle cells, chondrocytes and peripheral nerve fibers (Carriel et al. 2013; Garcia-Martinez et al. 2017; Mills 2012).

Other important molecules of the ECM are the proteoglycans. Our results showed that WJSC synthesized high amounts of these molecules as compared to FIB, showing an intercellular pattern in both cases. Our results demonstrated a high intrinsic capability of WJSC to synthesize ECM molecules during the MT-formation process. These results are supported by a recent study in which WJSC were cultured in flasks until they generated a membrane-like structure (14 ± 2 days) (Jaimes-Parra et al. 2017). Interestingly, these membranes resulted to be composed by WJSC organized around ECM-rich areas containing abundant collagens and proteoglycans (Jaimes-Parra et al. 2017). The particular pattern observed in these membranes was similar to the peripheral 3D organization that our WJSC acquired during the MT-formation process. The particular peripheral pattern characterizing the WJSC-MT could be related to several factors, such as a high cell proliferation rate and metabolic requirements.

An interesting previously known phenomenon is that epidermoid tumor cells injected in the subcutaneous tissue of nude mice tend to create solid tumors. In these cases, histology revealed proliferating and invading tumor cells in the tumor–host limits, while the inner part was mainly composed by less active cells and necrotic areas (Shen et al. 2018). Similarly, in tumor–stroma spheroids co-culture, it was demonstrated that proliferating cells were allocated at the spheroid surface, followed by quiescent cells, a hypoxic zone and a necrotic core (Horman et al. 2017). Both studies demonstrated that proliferating and metabolically active cells tend to adopt a superficial distribution to have preferential access to nutrients and oxygen exchange. In the present study, our results suggest that WJSC-MT have high capability to produce ECM components along with a high cellular metabolism. The continuous synthesis of ECM molecules could increase the energy requirements of the WJSC during MT-formation. Therefore, cells could progressively adopt a peripheral organization to ensure a continuous access to nutrients and oxygen, which in this ex vivo model must be obtained at the MT surface.

The ECM generated by human cells could be used as scaffolds for the generation of functional and biomimetic tissue-like substitutes by TE (Carriel et al. 2014; Philips et al. 2018). It is well-known that ECM molecules can modulate different kinds of cellular processes such as cell-attachment, migration, proliferation, morphogenesis, and differentiation (Godoy-Guzman et al. 2018; Rozario and DeSimone 2010). Therefore, native ECM is commonly used to build 3D scaffolds or to improve the biological properties of synthetic polymers (Campos et al. 2017; Carriel et al. 2014; Williams 2014). Based on this information, we hypothesize that the presence of an abundant ECM-rich core in WJSC-MT could contribute to improve the biomimicry and biological properties of bioengineered tissue-like substitutes. However, new studies are needed to demonstrate the cellular and molecular mechanisms related to the synthesis of an ECM-rich core, the particular peripheral 3D organization acquired by the WJSC during MT-formation and the potential usefulness of the WJSC-MT in TE.

As described above, the use of WJSC-MT could have potential clinical applications that should be determined by future works. In addition to their proliferation and differentiation potential, WJSC can be obtained from tissues frequently discarded at birth. Form a clinical point of view, these cells have been used in a wide range of clinical trials to treat different kinds of pathological conditions (e.g., autoimmune, hematological, neurodegenerative and orthopedics issues) with promising results (Davies et al. 2017; Kalaszczynska and Ferdyn 2015). Now, we demonstrated that these cells can synthetize abundant ECM components that could increase their usefulness in definite applications.

In conclusion, this ex vivo study demonstrated the suitability of WJSC to generate structurally stable MT using agarose microchips, with maximum viability and metabolic activity found between 4 and 21 days of EVD. In summary, we hypothesize that WJSC-MT could be a promising alternative for the generation of natural, functional and ECM-rich substitutes for potential TE applications. However, further research is still needed to demonstrate the ex vivo multipotent differentiation capability of WJSC-MT and their potential usefulness to promote tissue regeneration in in vivo models.

Acknowledgements This study was supported by the Spanish plan Nacional de investigación Científica, Desarrollo e Innovación Tecnológica, Ministry of Economy and Competitiveness (Instituto de Salud Carlos III), Grant Nos. FIS PI17/393 and FIS PI17/391, co-financed by Fondo Europeo de Desarrollo Regional (ERDF-FEDER, EU), UE and by the Regional Ministry of Health, Junta de Andalucía, Spain, Grant Nos. SAS PI-400-2016 and CS PI-0257-2017. Authors are grateful to Dr. Ariane Ruyffelaert for the editing language service.

Daniel Durand was supported by "Consejo Nacional de Ciencia y Tecnología" (CONACYT), scholarship program from Mexican government 580680/694261. Finally, this study forms part of the Doctoral Thesis of Daniel Durand Herrera.

References

Achilli TM, Meyer J, Morgan JR (2012) Advances in the formation, use and understanding of multi-cellular spheroids. Expert Opin Biol Therapy 12:1347–1360. https://doi.org/10.1517/14712598.2012.707181

Al Madhoun A, Ali H, AlKandari S, Atizado VL, Akhter N, Al-Mulla F, Atari M (2016) Defined three-dimensional culture conditions mediate efficient induction of definitive endoderm lineage from human umbilical cord Wharton's jelly mesenchymal stem cells. Stem Cell Res Therapy 7:165. https://doi.org/10.1186/s13287-016-0426-9

Alaminos M, Del Carmen Sanchez-Quevedo M, Munoz-Avila JI, Serrano D, Medialdea S, Carreras I, Campos A (2006) Construction of a complete rabbit cornea substitute using a fibrin-agarose scaffold. Investig Ophthalmol Vis Sci 47:3311–3317. https://doi.org/10.1167/iovs.05-1647

Atala A (2012) Regenerative medicine strategies. J Pediatric Surg 47:17–28. https://doi.org/10.1016/j.jpedsurg.2011.10.013

Berneel E, Philips C, Declercq H, Cornelissen R (2016) Redifferentiation of High-throughput generated fibrochondrocyte microaggregates: impact of low oxygen tension. Cells Tissues Organs https://doi.org/10.1159/000447509

Campos F et al (2016) Ex vivo characterization of a novel tissue-like cross-linked fibrin-agarose hydrogel for tissue engineering applications. Biomed Mater 11:055004. https://doi.org/10.1088/1748-6041/11/5/055004

Campos F et al. (2017) Generation of genipin cross-linked fibrin-agarose hydrogels tissue-like models for tissue engineering applications. Biomed Mater. https://doi.org/10.1088/1748-605X/aa9ad2

Carriel VGI (2009) Aplicación del método de bolque celular para evaluar la población de fibroblastos de mucosa oral en ingeniería tisular. Actual Med 94/2009:007–011

Carriel V, Garzon I, Alaminos M, Campos A (2011a) Evaluation of myelin sheath and collagen reorganization pattern in a model of peripheral nerve regeneration using an integrated histochemical approach. Histochem Cell Biol 136:709–717. https://doi.org/10.1007/s00418-011-0874-3

Carriel VS, Aneiros-Fernandez J, Arias-Santiago S, Garzon IJ, Alaminos M, Campos A (2011b) A novel histochemical method for a simultaneous staining of melanin and collagen fibers. J Histochem Cytochem 59:270–277. https://doi.org/10.1369/0022155410398001

Carriel V et al. (2012) Epithelial and stromal developmental patterns in a novel substitute of the human skin generated with fibrin-agarose biomaterials. Cells Tissues Organs 196:1–12 https://doi.org/10.1159/000330682

Carriel V et al (2013) Combination of fibrin-agarose hydrogels and adipose-derived mesenchymal stem cells for peripheral nerve regeneration. J Neural Eng 10:026022. https://doi.org/10.1088/1741-2560/10/2/026022

Carriel V, Alaminos M, Garzon I, Campos A, Cornelissen M (2014) Tissue engineering of the peripheral nervous system. Expert Rev Neurother 14:301–318. https://doi.org/10.1586/14737175.2014.887444

Carriel V et al (2015) In vitro characterization of a nanostructured fibrin agarose bio-artificial nerve substitute. J Tissue Eng Regen Med. https://doi.org/10.1002/term.2039

Carriel V, Garzon I, Campos A, Cornelissen M, Alaminos M (2017) Differential expression of GAP-43 and neurofilament during peripheral nerve regeneration through bio-artificial conduits. J Tissue Eng Regen Med 11:553–563. https://doi.org/10.1002/term.1949

Davies JE, Walker JT, Keating A (2017) Concise review: Wharton's jelly: the rich, but enigmatic, source of mesenchymal stromal cells. Stem Cells Transl Med. https://doi.org/10.1002/sctm.16-0492

Dean DM, Napolitano AP, Youssef J, Morgan JR (2007) Rods, tori, and honeycombs: the directed self-assembly of microtissues with prescribed microscale geometries. FASEB J 21:4005–4012. https://doi.org/10.1096/fj.07-8710com

Dominici M et al (2006) Minimal criteria for defining multipotent mesenchymal stromal cells. The International Society for Cellular Therapy position statement. Cytotherapy 8:315–317. https://doi.org/10.1080/14653240600855905

Donders R et al (2018) Human Wharton's jelly-derived stem cells display a distinct immunomodulatory and proregenerative transcriptional signature compared to bone marrow-derived stem cells. Stem Cells Dev 27:65–84. https://doi.org/10.1089/scd.2017.0029

Edmondson R, Adcock AF, Yang L (2016) Influence of matrices on 3D-cultured prostate cancer cells' drug response and expression of drug-action associated proteins. PloS One 11:e0158116. https://doi.org/10.1371/journal.pone.0158116

Fennema E, Rivron N, Rouwkema J, van Blitterswijk C, de Boer J (2013) Spheroid culture as a tool for creating 3D complex tissues. Trends Biotechnol 31:108–115. https://doi.org/10.1016/j.tibtech.2012.12.003

Fernandez-Valades-Gamez R et al. (2016) Usefulness of a bioengineered oral mucosa model for preventing palate bone alterations in rabbits with a mucoperiostial defect. Biomed Mater 11:015015. https://doi.org/10.1088/1748-6041/11/1/015015

Garcia-Martinez L et al (2017) Encapsulation of human elastic cartilage-derived chondrocytes in nanostructured fibrin-agarose hydrogels. Histochem Cell Biol 147:83–95. https://doi.org/10.1007/s00418-016-1485-9

Garzon I et al (2012a) A combined approach for the assessment of cell viability and cell functionality of human fibrochondrocytes for use in tissue engineering. PloS One 7:e51961. https://doi.org/10.1371/journal.pone.0051961

Garzon I et al (2012b) Evaluation of the cell viability of human Wharton's jelly stem cells for use in cell therapy. Tissue Eng Part C Methods 18:408–419. https://doi.org/10.1089/ten.TEC.2011.0508

Garzon I et al (2014a) Expression of epithelial markers by human umbilical cord stem cells. A topographical analysis. Placenta 35:994–1000. https://doi.org/10.1016/j.placenta.2014.09.007

Garzon I et al (2014b) Generation of a biomimetic human artificial cornea model using Wharton's jelly mesenchymal stem cells. Investig Ophthalmol Vis Sci 55:4073–4083. https://doi.org/10.1167/iovs.14-14304

Godoy-Guzman C, Nunez C, Orihuela P, Campos A, Carriel V (2018) Distribution of extracellular matrix molecules in human uterine tubes during the menstrual cycle: a histological and immunohistochemical analysis. J Anat. https://doi.org/10.1111/joa.12814

Horman SR et al (2017) Functional profiling of microtumors to identify cancer associated fibroblast-derived drug targets. Oncotarget 8:99913–99930. https://doi.org/10.18632/oncotarget.21915

Jaimes-Parra BD et al (2017) Membranes derived from human umbilical cord Wharton's jelly stem cells as novel bioengineered tissue-like constructs. Histol Histopathol. https://doi.org/10.14670/HH-11-897

Kalaszczynska I, Ferdyn K (2015) Wharton's jelly derived mesenchymal stem cells: future of regenerative medicine? Recent findings and clinical significance. BioMed Res Int 2015:430847. https://doi.org/10.1155/2015/430847

Kiernan JA (2008) Histological and histochemical methods: theory and practice, 4th edn. Scion, Oxford

Krotz SP, Robins JC, Ferruccio TM, Moore R, Steinhoff MM, Morgan JR, Carson S (2010) In vitro maturation of oocytes via the prefabricated self-assembled artificial human ovary. J Assist Reprod Genet 27:743–750. https://doi.org/10.1007/s10815-010-9468-6

Martin-Piedra MA, Garzon I, Oliveira AC, Alfonso-Rodriguez CA, Carriel V, Scionti G, Alaminos M (2014) Cell viability and proliferation capability of long-term human dental pulp stem cell cultures. Cytotherapy 16:266–277. https://doi.org/10.1016/j.jcyt.2013.10.016

Mills SE (2012) Histology for pathologists/editor: Stacey E. Mills, 4th edn. edn. Lippincott Williams & Wilkins, Philadelphia

Napolitano AP, Chai P, Dean DM, Morgan JR (2007a) Dynamics of the self-assembly of complex cellular aggregates on micromolded nonadhesive hydrogels. Tissue Eng 13:2087–2094. https://doi.org/10.1089/ten.2006.0190

Napolitano AP et al. (2007b) Scaffold-free three-dimensional cell culture utilizing micromolded nonadhesive hydrogels. BioTechniques 43:494, 496–500

Philips C, Cornelissen M, Carriel V (2018) Evaluation methods as quality control in the generation of decellularized peripheral nerve allografts. J Neural Eng 15:021003. https://doi.org/10.1088/1741-2552/aaa21a

Potier E, Rivron NC, Van Blitterswijk CA, Ito K (2016) Micro-aggregates do not influence bone marrow stromal cell chondrogenesis. J Tissue Eng Regen Med 10:1021–1032. https://doi.org/10.1002/term.1887

Rodriguez-Arco L et al (2016) Biocompatible magnetic core-shell nanocomposites for engineered magnetic tissues. Nanoscale 8:8138–8150. https://doi.org/10.1039/c6nr00224b

Roosens A, Puype I, Cornelissen R (2017) Scaffold-free high throughput generation of quiescent valvular microtissues. J Mol Cell Cardiol 106:45–54. https://doi.org/10.1016/j.yjmcc.2017.03.004

Rozario T, DeSimone DW (2010) The extracellular matrix in development and morphogenesis: a dynamic view. Dev Biol 341:126–140. https://doi.org/10.1016/j.ydbio.2009.10.026

Schugar RC et al (2009) High harvest yield, high expansion, and phenotype stability of CD146 mesenchymal stromal cells from whole primitive human umbilical cord tissue. J Biomed Biotechnol 2009:789526. https://doi.org/10.1155/2009/789526

Shen YQ et al. (2018) Combination of melatonin and rapamycin for head and neck cancer therapy: suppression of AKT/mTOR pathway activation, and activation of mitophagy and apoptosis via mitochondrial function regulation J Pineal Res. https://doi.org/10.1111/jpi.12461

Song W et al (2016) Dynamic self-organization of microwell-aggregated cellular mixtures. Soft Matter 12:5739–5746. https://doi.org/10.1039/c6sm00456c

Taghizadeh RR, Cetrulo KJ, Cetrulo CL (2011) Wharton's Jelly stem cells: future clinical applications. Placenta 32(Suppl 4):S311–S315. https://doi.org/10.1016/j.placenta.2011.06.010

Talaei-Khozani T, Borhani-Haghighi M, Ayatollahi M, Vojdani Z (2015) An in vitro model for hepatocyte-like cell differentiation from Wharton's jelly derived-mesenchymal stem cells by cell-base aggregates Gastroenterol Hepatol Bed Bench 8:188–199

Williams DF (2014) The biomaterials conundrum in tissue engineering. Tissue Eng Part A 20:1129–1131. https://doi.org/10.1089/ten.tea.2013.0769

Zorlutuna P et al (2012) Microfabricated biomaterials for engineering 3D tissues. Adv Mater 24:1782–1804. https://doi.org/10.1002/adma.201104631